Supporting Information

Single-molecule analyte recognition with ClyA nanopores equipped with internal protein adaptors

Misha Soskine[1,2*], Annemie Biesemans[2,*] and Giovanni Maglia[1,2]

[1]Department of Chemistry, University of Leuven, Leuven, 3001, Belgium

[2]Groningen Biomolecular Sciences & Biotechnology (GBB) Institute, University of Groningen, 9747 AG, Groningen, The Netherlands

[*]These authors contributed equally to the work

Keywords: ClyA, nanopore sensing, enzymology, single-molecule, AlkB, DHFR

[2]Correspondence to: g.maglia@rug.nl

Giovanni Maglia, PhD

Professor of Chemical Biology

University of Groningen

Groningen Biomolecular Sciences & Biotechnology (GBB) Institute

Nijenborgh 7, 9747 AG

PO Box 11103, 9700 CC

Groningen, The Netherlands

Phone: +31(0)50 363 6138

Additional text

AlkB blockades

About 30% of the AlkB-Fe^{++}-induced current blockades did not show ligand-induced transitions, suggesting that the trapped enzymes might have a preferred orientation inside the ClyA-AS lumen. An alternative explanation is that sub-populations of AlkB-Fe^{++} might be inactive as a consequence of self-inactivation,[1] proteolysis, loss of iron, misfolding, etc. AlkB blockades not showing ligand-induced current transitions were ignored and the enzyme was ejected from the pore by reversing the potential to +60 mV. The AlkB-Fe^{++} blockades were nearly eliminated upon addition of 40 μM of cognate aptamer (Figure S6, Table S5), indicating that, as previously reported for other proteins,[2] AlkB-Fe^{++} formed complexes with the aptamer, which cannot be captured by ClyA nanopores as a result of electrostatic repulsion and/or steric hindrance.[3] This suggests that the majority of captured AlkB proteins are natively folded, as such aptamer was evolved to bind to folded AlkB.[4]

Heterogeneities in $DHFR_{tag}$:MTX blockades and NAPDH binding events

Approximately 45% of the $DHFR_{tag}$:MTX blockades did not respond to the addition of NADP+ (added in *trans*, Figure S7c,d). Since all the observed $DHFR_{tag}$ molecules captured by ClyA-AS were bound to MTX, this effect is not likely due to misfolded DHFR molecules. Besides, when NADPH was added to the *trans* chamber, two distinct populations of $DHFR_{tag}$:MTX blockades were observed: the first (~55% of blockades) gave rise to NADPH binding events with a lifetime longer than the residence time of the complex within ClyA-AS (lifetime >3 seconds, “long” NADPH events), the second population (~45% of blockades) corresponded to $DHFR_{tag}$:MTX blockades that displayed NADPH binding events with a lifetime of 38.5±0.8 ms (“short” NADPH events). Most blockades showed either “long” or ”short” NADPH events (Figure S7a). Rarely, however, the same $DHFR_{tag}$:MTX blockade switched between the two NADPH binding behaviours (Figure S7b). “Long” and ”short” NADPH events showed similar association rate constants (k_{on} = 4.8 ±1.2 $s^{-1}\mu M^{-1}$ and k_{on} = 5.8±1.2 $s^{-1}\mu M^{-1}$, respectively) and comparable $\Delta_{IRES\%}$ values (2.7±0.7% and 2.2±0.9%, respectively, Figure S7a,b). Although “short” NADPH binding events could arise from NADP+ contaminations, this is unlikely since fresh NADPH aliquots (>95% purity) were used for every experiment. Furthermore, the lifetime of “short” NADPH events was significantly shorter than the lifetime of NADP+ events. In addition, the fact that most of the $DHFR_{tag}$:MTX blockades showed only one binding behaviour suggests that the

observed heterogeneity is not arising from impurities in the substrate samples but from heterogeneity in the protein adaptor (Figure S7). This variability in binding behaviour could then arise from different configurations of $DHFR_{tag}$:MTX inside the ClyA-AS nanopore and/or from different conformations of the $DHFR_{tag}$:MTX complex. Although the first hypothesis cannot be easily tested, it is interesting to note that previous studies revealed that MTX can bind to two different DHFR conformations with different binding affinities towards NADP+ and NADPH.[5]

Tailoring the DHFR nanopore adaptor for optimal nanopore residence

Our initial DHFR construct (named apo-DHFR in main text and DHFR in SI) consisted of DHFR from *E. coli* with the cysteine residues at positions 85 and 152 substituted with alanine and serine, respectively, and with a C-terminal Strep-tag, inserted for purification purposes, spaced by a 9 amino acid long linker (see later). The fusion tag polypeptide chain contained one additional net positive charge with respect to the wild type sequence (originating from the introduction of a Xho I restriction site in the DNA sequence of the protein, Figure S4). The addition of apoDHFR (50 nM, Figure S4) to the *cis* compartment induced transient blockades to the ClyA-AS open pore current with $I_{RES\%}$ of 71.5±0.8 % and a lifetime of 21±2 ms (n_p=200 blockades, N=4 single channels) under –90 mV applied potential (Figure S4a, left). Subsequent addition of 400 nM of MTX to the *cis* compartment resulted in blockades with increased $I_{RES\%}$ values ($I_{RES\%}$=78.4±0.6%) and decreased lifetime (3.3±0.7 ms, n_p=300 blockades, N=3 single channels, Figure S3a, centre). Further addition of 20 μM NADPH to the same compartment resulted in the nearly total elimination of the DHFR blockades (Figure S4a, right), suggesting that the DHFR:MTX:NADPH complex was mostly excluded from the ClyA-AS nanopore. Thus, although we could observe the interaction between the ligands and DHFR, the protein did not remain inside the ClyA-AS nanopore for a time long enough to determine the binding kinetics, prompting us to design DHFR constructs that would have a longer residence time within the ClyA-AS nanopore.

In order to increase the residence time of DHFR into ClyA, we have designed and tested three DHFR constructs that were decorated with a different number of positive charges incorporated into flexible C-terminal fusion tags. We expected that the additional charges would prolong the dwell times of the ternary complex within the ClyA-AS nanopore because of the decreased electrostatic repulsion between the negatively charged protein (the theoretical pI of DHFR is 4.8) and the negatively charged nanopore lumen,[6] and the reduced electrophoretic drag on DHFR under negative applied potentials. Initially we tested $DHFR_{10+}$, which consisted of the

DHFR gene with a C-terminal recombinant tag baring 10 net positive charges with respect to wild type DHFR. The sequence of the 10+ tag comprised of a S-tag (KETAAAKFERQHMDS) derived from pancreatic RNase A, followed by a positively charged coil (KIAALKQKIAALKYKNAALKKKIAALKQ, adapted from[7]) and, a Strep-tag for purification. DHFR and the three tags were spaced by flexible linkers (Figure S4). Since we could not predict what would be the effect of the positively charged tag and linker length on the DHFR blockades, we have also designed two constructs with shorter tags and smaller number of additional positive charges: $DHFR_{4+}$ and $DHFR_{tag}$ baring 4 and 5 net positive charges, respectively (Figure S4). $DHFR_{10+}$, $DHFR_{4+}$ and $DHFR_{tag}$ induced fast current blockades to ClyA-AS nanopores that converted into second-long blockades upon binding to MTX (Figure S3). $DHFR_{10+/4+/tag}$:MTX blockades were remarkably longer than DHFR:MTX blockades (e.g. the lifetime of $DHFR_{tag}$:MTX blockades was ~1000 fold that of DHFR:MTX blockades), indicating that the positively charged tags efficiently counterbalanced the electrostatic and electrophoretic effects induced by MTX binding (Figure S3). Although the blockades induced by the $DHFR_{10+/4+/tag}$:MTX complexes reported the binding of NADPH through ~4 pA enhancements of the residual ionic current (Figure S3b,c,d, right), $DHFR_{10+}$ and $DHFR_{4+}$ blockades produced non-ideal output signals. The residual current of $DHFR_{10+}$ blockades often switched to a level of lower conductance (Figure S3b, centre and right), while the binding of NADPH to $DHFR_{4+}$:MTX prompted the quick release of the complex from the pore, indicating that 4 additional positive charges are not enough to keep the ternary complex within the pore (Figure S3c, right). On the other hand, $DHFR_{tag}$:MTX:NADPH was internalised for sufficient time for accurate kinetic analysis and therefore it was chosen for thorough characterization as our nanopore-adaptor.

AlkB and DHFR mode of detection

AlkB and DHFR were selected as protein adaptors because they both undergo a large conformational transitions upon binding to their substrates and cofactors.[8-12] Therefore, it is possible that the residual current transitions observed in the presence of ligands reflect the conformational changes of the confined enzyme molecules. However, other possible explainations exist. For example, the ligands possess multiple net negative charges (two for 2-OG, SUC and N-OG, three for NADP+ and four for NADPH), thus it is possible that the binding of the substrate influences the residual current by changing the configuration or position of the confined enzyme molecule within ClyA. More complex interactions between the nanopore internal surface and the confined protein adaptor cannot be excluded.

Furthermore, when apoAlkB-Fe^{++} was confined inside ClyA, short-living current enhancements were observed in the absence of added ligands. Upon the addition of ligands the current enhancements became much longer duration and showed a well defined current level (Figure S1). It is possible therefore that AlkB lingads are recognized with a molecular recognition mechanism based on conformational selection, in which ligands selectively bind to a pre-existing conformational state of the protein that is only lowly populated and short living in the absence of the ligand.[13] The binding of ligands will then merely result in an increased lifetime of this pre-existing closed state. Alternatively, the protein adaptor might interact with the nanopore walls. Then the binding of the ligands to the protein adaptor might change the interaction between the pore and the adaptor.

Materials and methods

Unless otherwise specified all chemicals were bought from Sigma-Aldrich. DNA was purchased from Integrated DNA Technologies (IDT), enzymes from Fermentas and lipids from Avanti Polar Lipids. Stocks of NADPH and NADP+ (prepared in 15 mM Tris.HCl pH 7.5 150 mM NaCl) were kept at -20 ºC and defrosted for single use. All errors in this work are given as standard deviations. The standard deviations (SD) for the values calculated from linear fits (Figure 2b, Figure 4b in main text) were calculated from standard errors (SE) given by the fit by applying the formula $SE = \frac{SD}{\sqrt{N}}$ where N is the number of independent data points in the graph.

AlkB cloning

To allow cloning, a Nco I site (CCATGG) was introduced in the wild type AlkB from *E. coli* at the beginning of the gene (5' end). To keep the gene in reading frame an additional two bases were inserted after the Nco I site, resulting in an additional alanine residue after the starting methionine. For purification purposes, at the C-terminus of AlkB, a strep-tag was attached via a flexible glycine-serine-alanine linker and the open reading frame was terminated by two consecutive stop codons, followed by a Hind III restriction site (3' end). The attachment of the strep-tag was carried out in two consecutive PCR reactions. During the first PCR reaction, the AlkB gene was amplified directly from the genomic DNA of a single BL21(DE3) *E. coli* (Lucigen) colony using Phire Hot Start II DNA polymerase (Finnzymes), 6 μM fAlkB (Table S5) and AlkBr1 (Table S5) primers in a 50 μL reaction volume. The PCR reaction cycling protocol was as follows: pre-incubation step at 98ºC for 30 s and then 30 cycles of denaturation at 98ºC for 5 s

and extension at 72ºC for 1 min. The amplified product was purified using QIAquick PCR Purification Kit (Qiagen) and served as a template for the second PCR reaction, which used ~100 ng of the purified PCR product amplified by Phire Hot Start II DNA polymerase using 6 μM of fAlkB (Table S5) and AlkBr2 (Table S5) primers in 300 μL volume. The cycling protocol was the same as in the previous step. The resulting PCR product containing the strep-tagged AlkB gene was purified with QIAquick PCR Purification Kit (Qiagen) and digested with Nco I and Hind III (FastDigest, Fermentas). The gel purified insert (QIAquick Gel Extraction Kit, Qiagen) was cloned under control of the T7 promoter into the pT7-SC1 expression plasmid[15] using sticky-end ligation (T4 ligase, Fermentas) via Nco I (5') and Hind III (3') sites. 0.6 μL of the ligation mixture was transformed into 50 μL of E. cloni® 10G cells (Lucigen) by electroporation. The transformed bacteria were grown overnight at 37ºC on ampicillin (100 μg/ml) LB agar plates. The identity of the clones was confirmed by sequencing. The DNA and proteins sequences of strep-tagged AlkB are given below.

>AlkB-streptag (protein sequence, additional amino acid residues are underlined)
MALDLFADAEPWQEPLAAGAVILRRFAFNAAEQLIRDINDVASQSPFRQMVTPGGYTMSVAMT
NCGHLGWTTHRQGYLYSPIDPQTNKPWPAMPQSFHNLCQRAATAAGYPDFQPDACLINRYAP
GAKLSLHQDKDEPDLRAPIVSVSLGLPAIFQFGGLKRNDPLKRLLLEHGDVVVWGGESRLFYH
GIQPLKAGFHPLTIDCRYNLTFRQAGKKEGSAWSHPQFEK**

>AlkB-streptag (DNA sequence)
atggcgttggatctgtttgccgatgctgaaccgtggcaagagccactggcggctggtgcggtaattttacggcgttttgcttttaacgctgc
ggagcaactgatccgcgatattaatgacgttgccagccagtcgccgtttcgccagatggtcacccccgggggatataccatgtcggtg
gcgatgaccaactgtgggcatctgggctggacgacccatcggcaaggttatctctattcgcccattgatccgcaaacaaataaaccgt
ggcccgccatgccacagagttttcataatttatgtcaacgtgcggctacggcggcgggctatccagatttccagccagatgcttgtcttat
caaccgctacgctcctggcgcgaaactgtcgctgcatcaggataaagacgaaccggatctgcgcgcgccaattgtttctgtttctctgg
gcttacccgcgatttttcaatttggcggcctgaaacgaaatgatccgctcaaacgtttgttgttggaacatggcgatgtggtggtatgggg
cggtgaatcgcggctgttttatcacggtattcaaccgttgaaagcggggtttcatccactcaccatcgactgccgctacaacctgacattc
cgtcaggcaggtaaaaaagaaggcagcgcgtggagccatccgcagtttgaaaaatgatAAGCTT

Construction of the DHFR$_{n+}$ genes

The synthetic gene encoding for *E. coli* DHFR was made by GenScript. The wild-type gene was modified by the substitution of the two Cys residues at positions 85 and 152 with Ala and Ser respectively (referred to as DHFR throughout SI and main text). Those substitutions were shown to be functionally tolerated by DHFR.[14] Further, the DNA sequence encoding for Met-Ala-

Ser-Ala was added at the beginning of the gene in order to introduce a Nco I restriction site. To facilitate construction steps, a Xho I restriction site was introduced between the C-terminal tags and DHFR.

As a first step the $DHFR_{10+}$ construct was built (Figure S4, for DNA and protein sequences see below). 100 ng of the synthetic DHFR gene was amplified with 5 µM of DHf and DHr primers (Table S5) with Phire Hot Start II DNA polymerase (Finnzymes) in 400 µL final volume (pre-incubation at 98ºC for 30s, then cycling: denaturation at 98ºC for 5 s, extension at 72ºC for 1 min for 30 cycles). The synthetic fragment encoding for the 10+ tag (made by IDT, for sequence see below) was amplified as described above using Cof and Cor primers (Table S5). DHf and Cof primers contain sequences that are the reverse-complement of each other, introducing sequence overlap between DHFR and 10+ tag PCR products, necessary for the next step, where both PCR products (2 µg each, gel-purified, QIAquick Gel Extraction Kit, Qiagen) were assembled together using Phire Hot Start II DNA polymerase (Finnzymes) in 50 µL final volume (pre-incubation at 98ºC for 30s, then cycling: denaturation at 98ºC for 5 s, extension at 72ºC for 1 min for 7 cycles). ~100 ng of the purified (QIAquick PCR Purification Kit (Qiagen)) assembly product was amplified with 5 µM of DHf and Cor primers (Table S5), using Phire Hot Start II DNA polymerase (Finnzymes) in 400 µL final volume (pre-incubation at 98ºC for 30s, then cycling: denaturation at 98ºC for 5 s, extension at 72ºC for 1 min for 30 cycles). PCR product encoding for the whole length $DHFR_{10+}$ was purified using the QIAquick PCR Purification Kit (Qiagen) and digested with Nco I and Hind III (FastDigest, Fermentas). The resulting insert was gel purified and cloned under control of the T7 promoter into the pT7-SC1 expression plasmidusing sticky-end ligation (T4 ligase, Fermentas) via Nco I (5') and Hind III (3') sites. 0.6 µL of the ligation mixture was transformed into E. cloni® 10G cells (Lucigen) by electroporation. The transformed bacteria were selected overnight at 37ºC on ampicillin (100 µg/ml) LB agar plates. The identity of the clones was confirmed by sequencing. The DNA and protein sequence of $DHFR_{10+}$ is provided below with the 10+ tag sequence indicated by capital letters in the DNA sequence.

> $DHFR_{10+}$ (DNA sequence)

atggcttcggctatgatttctctgattgcggcactggctgtcgatcgtgttattggtatggaaaacgctatgccgtggaatctgccggctgat
ctggcgtggtttaaacgtaacactctggacaagccggtcattatgggccgccatacgtgggaaagcatcggtcgtccgctgccgggtc
gcaaaaatattatcctgagcagccagccgggcaccgatgaccgtgtgacgtgggttaagagcgtcgatgaagcaattgcggcggca
ggcgacgtgccggaaattatggttatcggcggtggccgcgtttatgaacagttcctgccgaaagcccaaaagctgtacctgacccata
tcgatgcagaagtcgaaggtgatacgcactttccggactatgaaccggatgactgggaaagtgtgttctccgaatttcacgacgccga

cgctcagaacagccactcatactcattcgaaatcctggaacgccgtGGCAGCAGTACTCGAGCGAAAGAAACCG
CGGCGGCGAAATTTGAACGCCAGCATATGGATAGCGGCAGCGCGAAAATTGCCGCACTTA
AACAAAAAATCGCGGCGCTGAAGTATAAAAATGCGGCACTAAAAAAGAAGATTGCGGCCCT
AAAACAGGGCAGCGCGTGGAGCCATCCGCAGTTTGAAAAATGATAAGCTTGGA

> $DHFR_{10+}$ (protein sequence, additional amino acid residues are underlined)
MASAMISLIAALAVDRVIGMENAMPWNLPADLAWFKRNTLDKPVIMGRHTWESIGRPLPGRKNI
ILSSQPGTDDRVTWVKSVDEAIAAAGDVPEIMVIGGGRVYEQFLPKAQKLYLTHIDAEVEGDTH
FPDYEPDDWESVFSEFHDADAQNSHSYSFEILERRGSSTRAKETAAAKFERQHMDSGSAKIAA
LKQKIAALKYKNAALKKKIAALKQGSAWSHPQFEK**

DHFR, $DHFR_{4+}$ and $DHFR_{tag}$ constructs (Figure S4) were built by deleting parts of the 10+ tag via whole plasmid PCR amplification followed by Xho I digestion and unimolecular ligation as follows: ~100 ng of the DHFR_10+ tag plasmid was amplified using 5 μM of dcr and delF (to produce DHFR), or 2dcF ($DHFR_{4+}$) or dcf ($DHFR_{tag}$) using Phire Hot Start II DNA polymerase (Finnzymes) in 100 μL final volume (pre-incubation at 98ºC for 30s, then cycling: denaturation at 98ºC for 5 s, extension at 72ºC for 1.5 min for 30 cycles, primer sequences see Table S5). PCR products were purified with QIAquick PCR Purification Kit (Qiagen), digested with Xho I (FastDigest, Fermentas) and ligated with T4 ligase (Fermentas). 0.6 μL of the ligation mixture was transformed into E. cloni® 10G cells (Lucigen) by electroporation. The transformed bacteria were selected overnight at 37ºC on ampicillin (100 μg/ml) LB agar plates. The identity of the clones was confirmed by sequencing.

Construction of N120D AlkB mutant

The AlkB gene was amplified using 120D (forward) and T7 terminator (reverse) primers (Table S5). The PCR conditions were: 0.3 mL final volume of PCR mix (150 μl of RED Taq ReadyMix, 6 μM of forward and reverse primers, ~400 ng of template plasmid), cycled for 27 times (after a pre-incubation step at 95ºC for 3 min, a cycling protocol was then applied: denaturation at 95ºC for 15 s, annealing at 55ºC for 15 s, extension at 72ºC for 3 min). The resulting PCR product was gel purified (QIAquick Gel Extraction Kit, Qiagen) and cloned into a pT7 expression plasmid (pT7-SC1) by MEGAWHOP procedure:[16] ~500 ng of the purified PCR product was mixed with ~300 ng of the WT AlkB circular DNA template and the amplification was carried out with Phire

Hot Start II DNA polymerase (Finnzymes) in 50 µL final volume (pre-incubation at 98ºC for 30s, then cycling: denaturation at 98ºC for 5 s, extension at 72ºC for 1.5 min for 30 cycles). The circular template was eliminated by incubation with Dpn I (1 FDU) for 2 hr at 37ºC. 0.6 µL of the resulted mixture was transformed into 50 µL of E. cloni® 10G cells (Lucigen) by electroporation. The transformed bacteria were grown overnight at 37ºC on ampicillin (100 µg/ml) LB agar plates. The identity of the clones was confirmed by sequencing.

Purification of the strep-tagged AlkB-Fe^{++}

pT7-SC1 plasmids containing the strep-tagged AlkB gene were transformed into E. cloni® EXPRESS BL21(DE3) cells (Lucigen). Transformants were selected on LB agar plates supplemented with 100 µg/ml ampicillin grown overnight at 37˚C. The resulting colonies were grown at 37˚C (200 rpm shaking) in 2xYT medium supplemented with 100 µg/ml ampicillin until the O.D. at 600 nm was ~ 0.8. The cultures were then supplemented with 25 µM $FeSO_4$ and 100 µM L(+)-ascorbic acid (Merck) from fresh stock solutions (25 mM $FeSO_4$ and 100 mM L(+)-ascorbic acid in ddH_2O) and the protein expression was induced by supplementing with 0.5 mM IPTG. Bacteria were further grown overnight at 25˚C, 200 rpm shaking. The next day the bacteria were harvested by centrifugation at 6000 x g at 4˚C for 25 min. The resulting pellets were frozen at -80˚C until further use.

AlkB-Fe^{++} was purified as following: bacterial pellets originating from 100 ml culture were resuspended in 30 ml lysis buffer (150 mM NaCl, 15 mM Tris.HCl pH 8.0, 1 mM $MgCl_2$, 0.2 units/ml DNase, 10 µg/ml lysozyme) supplemented with 5 µl β-mercaptoethanol (Merck) and 25 µM $FeSO_4$ and 100 µM L(+)-ascorbic acid, and incubated at RT for 20 min. Bacteria were further disrupted by probe sonication, and the crude lysate was clarified by centrifugation at 6000 x g at 4˚C for 30 min. The supernatant was allowed to bind to ~150 µl (bead volume) of Strep-Tactin® Sepharose® (IBA) pre-equilibrated with the wash buffer (150 mM NaCl, 15 mM Tris.HCl pH 8.0) supplemented with 25 µM $FeSO_4$ and 100 µM L(+)-ascorbic acid, for 1 hr at 4˚C ("end over end" mixing). Then the resin was loaded on a column (Micro Bio Spin, Bio-Rad) and washed with ~ 20 column volumes of the wash buffer supplemented with 25 µM $FeSO_4$ and 100 µM L(+)-ascorbic acid followed by ~ 3 column volumes of 150 mM NaCl, 15 mM Tris.HCl pH 8.0 (metal ions might interfere with the ClyA recordings, unpublished results, thus excess of iron was avoided). AlkB-Fe^{++} was subsequently eluted from the column in ~ 300 µl of elution buffer (150 mM NaCl, 15 mM Tris.HCl pH 8.0, 5 mM D-desthiobiotin (IBA)). Purified AlkB-Fe^{++} remained active for weeks, in agreement with the fact that self-inactivation of AlkB requires the

presence of 2-OG.[1] The concentration of AlkB-Fe^{++} was measured using Bradford assay and the purity was checked using a 12% SDS-PAGE (Figure S8).

Purification of the strep-tagged $DHFR_{n+}$

After transformation of pT7-SC1 plasmids containing the strep-tagged $DHFR_{n+}$ gene into E. cloni® EXPRESS BL21(DE3) cells (Lucigen), transformants were selected on LB agar plates supplemented with 100 µg/ml ampicillin after overnight growth at 37˚C. The resulting colonies were grown at 37˚C (200 rpm shaking) in 2xYT medium supplemented with 100 µg/ml ampicillin until the O.D. at 600 was ~ 0.8, after which $DHFR_{n+}$ expression was induced by addition of 0.5 mM IPTG, and subsequent switching to 25°C for overnight growth. The next day the bacteria were harvested by centrifugation at 6000 x g at 4˚C for 25 min and the resulting pellets were frozen at -80˚C until further use.

For purification, bacterial pellets originating from 100 ml culture were resuspended in 30 ml lysis buffer (150 mM NaCl, 15 mM Tris.HCl pH 7.5, 1 mM $MgCl_2$, 0.2 units/ml DNase, 10 µg/ml lysozyme) and incubated at RT for 20 min. Bacteria were further disrupted by probe sonication, and the crude lysate was clarified by centrifugation at 6000 x g at 4˚C for 30 min. The supernatant was allowed to bind to ~150 µl (bead volume) of Strep-Tactin® Sepharose® (IBA) pre-equilibrated with the wash buffer (150 mM NaCl, 15 mM Tris.HCl pH 7.5) - "end over end" mixing. The resin was then loaded on a column (Micro Bio Spin, Bio-Rad) and washed with ~ 20 column volumes of the wash buffer. $DHFR_{n+}$ was subsequently eluted from the column in ~ 300 µl of elution buffer (150 mM NaCl, 15 mM Tris.HCl pH 7.5, 5 mM D-Desthiobiotin (IBA)). The concentration of $DHFR_{n+}$ was measured using Bradford assay and the purity was checked using a 12% SDS-PAGE (Figure S9). Proteins were stored at 4°C (up to 3 weeks) until use.

ClyA-AS protein overexpression and purification

E. cloni® EXPRESS BL21 (DE3) cells were transformed with the pT7-SC1 plasmid containing the ClyA-AS gene. ClyA-AS contains eight mutations relative to the *S. Typhi* ClyA-WT: C87A, L99Q, E103G, F166Y, I203V, C285S, K294R and H307Y (the H307Y mutation is in the C-terminal hexahistidine-tag added for purification).[6] Transformants were selected after overnight growth at 37ºC on LB agar plates supplemented with 100 mg/L ampicillin. The resulting colonies were inoculated into 2xYT medium containing 100 mg/L of ampicillin. The culture was grown at 37ºC, with shaking at 200 rpm, until it reached an OD_{600} of ~ 0.8. The expression of ClyA-AS was then induced by the addition of 0.5 mM IPTG and the growth was continued at 25ºC. The

next day the bacteria were harvested by centrifugation at 6000 x g for 25 min at 4°C and the pellets were stored at -80ºC.

The pellets containing monomeric ClyA-AS were thawed and resuspended in 20 mL of wash buffer (10 mM imidazole, 150 mM NaCl, 15 mM Tris.HCl, pH 8.0), supplemented with 1 mM $MgCl_2$ and 0.05 units/mL of DNase I and the bacteria were lysed by sonication. The crude lysates were clarified by centrifugation at 6000 x g for 20 min at 4°C and the supernatant was mixed with 200 μL of Ni-NTA resin (Qiagen) in wash buffer. After 1 hr, the resin was loaded into a column (Micro Bio Spin, Bio-Rad) and washed with ~5 ml of the wash buffer. ClyA-AS was eluted with approximately ~0.5 mL of wash buffer containing 300 mM imidazole. Protein concentration was determined by the Bradford assay. Because ClyA-AS monomers were not active upon freezing, they were stored at 4˚C until further use.

Type I ClyA-AS oligomers were obtained by incubation of ClyA-AS monomers with 0.5% β-dodecylmaltoside (DDM, GLYCON Biochemicals, GmbH) at 25ºC for 15 min. ClyA-AS oligomers were separated from monomers by blue native polyacrylamide gel electrophoresis (BN-PAGE, Bio-rad) using 4-20% polyacrylamide gels. The bands corresponding to Type I ClyA-AS were excised from the gel and were placed in 150 mM NaCl, 15 mM Tris.HCl pH 8.0 supplemented with 0.2% DDM and 10 mM EDTA to allow diffusion of the proteins out of the gel.

Electrical recordings in planar lipid bilayers

The applied potential refers to the potential of the *trans* electrode. ClyA-AS nanopores were inserted into lipid bilayers from the *cis* compartment, which was connected to the ground electrode. The two compartments were separated by a 25 μm thick polytetrafluoroethylene film (Goodfellow Cambridge Limited) containing an orifice of ~100 μm in diameter. The aperture was pretreated with ~5 μl of 10% hexadecane in pentane and a bilayer was formed by the addition of ~10 μL of 1,2-diphytanoyl-sn-glycero-3-phosphocholine (DPhPC) in pentane (10 mg/mL) to both electrophysiology chambers. Typically, the addition of 0.01-0.1 ng of oligomeric ClyA-AS to the *cis* compartment (0.5 mL) was sufficient to obtain a single channel. ClyA-AS nanopores displayed a higher open pore current at positive than at negative applied potentials, which provided a useful tool to determine the orientation of the pore. Electrical recordings were carried out in 150 mM NaCl, 15 mM Tris.HCl pH 8.0 (AlkB experiments) or 150 mM NaCl, 15 mM Tris.HCl pH 7.5 (DHFR experiments). The temperature of the recording chamber was maintained at 28°C by water circulating through a metal case in direct contact with the bottom and sides of the chamber.

Data recording and analysis

Electrical signals from planar bilayer recordings were amplified using an Axopatch 200B patch clamp amplifier (Axon Instruments) and digitized with a Digidata 1440 A/D converter (Axon Instruments). Data were recorded by using the Clampex 10.4 software (Molecular Devices) and the subsequent analysis was carried out with the Clampfit software (Molecular Devices). Electrical recordings were performed in 150 mM NaCl, 15 mM Tris.HCl pH 8.0 (AlkB) or pH 7.5 (DHFR) by applying a 2 kHz low-pass Bessel filter and a 10 kHz sampling rate. For further analysis traces were filtered digitally with a Bessel (8-pole) low-pass filter with a 50 Hz cut-off. Residual current values ($I_{RES\%}$) were calculated from blocked pore current values (I_B) and open pore current values (I_O) as $I_{RES\%} = 100 * I_B / I_O$. I_B and I_O were determined from Gaussian fits to all point current histograms (0.05 pA bin size) for at least 15 individual protein blockades. $\Delta I_{RES\%}$ values were calculated from $I_{RES\%}$ using propagation of errors.

Current transitions from level 1 were analyzed with the "single-channel search" function in Clampfit. The detection threshold to collect the ligand-induced events for AlkB was set to 4 pA and events shorter than 10 ms were ignored. For NADP+ and "short" NADPH binding events to $DHFR_{tag}$:MTX, the detection threshold was also set to 4 pA and events shorter than 1 ms were neglected. The resulting event dwell times (t_{off}) and the time between events (t_{on}) were binned together as cumulative distributions and fitted to a single exponential to retrieve the ligand-induced lifetimes ($\tau_{\mathbf{off}}$) and the ligand-induced event frequencies ($f = 1/\tau_{\mathbf{on}}$). The process of event collection was monitored manually. For AlkB, final values of $\tau_{\mathbf{on}}$ and $\tau_{\mathbf{off}}$ were based on average values derived from at least 3 single channel experiments at each concentration. Each experiment analysed more than 8 AlkB blockades. At the low ligand concentrations (0.2 mM) about 100 ligand-binding events were measured. Otherwise more than 150 events were collected. In total, 500 – 1200 events were considered for 2-OG, 350 – 2100 events for SUC (350 events were collected at the lowest concentration, all other concentrations more than 800 events) and 500 – 1300 events for N-OG. For $DHFR_{tag}$:MTX, >500 NADPH and >2000 NADP+ binding events were used in total to determine the values of $\tau_{\mathbf{on}}$ and $\tau_{\mathbf{off}}$, where individual values for t_{on} and t_{off} were derived from at least five single channel experiments, each analysing more than 40 $DHFR_{tag}$:MTX blockades and more than 2000 ligand-binding events. Since the life time of the "long" NADPH binding events to $DHFR_{tag}$:MTX binary complex exceeded the residence time of the binary complex in the ClyA-AS nanopore (the dissociation of NADPH was only occasionally observed), $t_{\mathbf{off}}$ values could not be determined. t_{on} values for NADPH were

determined by collecting the times between the capture of the $DHFR_{tag}$:MTX binary complex in the nanopore and the transition to the ~4 pA higher current level within the same blockade lasting longer than 0.2 s. Subsequently, the t_{on} values were binned together as cumulative distributions and fitted to a single exponential fit to retrieve characteristic τ_{on} values. The values for k_{off} represented in Figure 2b and Figure 4b were determined by taking the average ± standard deviations of $1/t_{off}$ of at least 3 single channel experiments. The values of the association rate constants (k_{on}) were determined from the slope of the linear regression curves calculated from the dependency of the event frequencies ($f = 1/\tau_{on}$) on the ligand concentration (OriginLab, Figure 2b and 4b). Graphs were made with Origin (OriginLab Corporation) or Clampfit software (Molecular Devices).

Table S1 | $I_{RES\%}$ values of AlkB-Fe^{++} ligand-induced current blockades. All data were collected at -60 mV applied potential in 150 mM NaCl, 15 mM Tris.HCl pH 8.0 at 28˚C. Values were calculated from 15 individual AlkB blockades. Errors are given as standard deviations. The ClyA-AS open-pore conductance (I_o) was 1.7±0.1 nSi (N=38 single channels). $\Delta I_{RES\%}$ is the difference between the $I_{RES\%}$ of the AlkB-Fe^{++} protein blockades and the $I_{RES\%}$ induced by the ligand (L1B or L2B). Proteins and ligands were added to the *cis* chamber.

	No ligand		**2-OG**		**SUC**		**N-OG**	
	L1 $I_{RES\%}$	**L2** $I_{RES\%}$	**L1B** $\Delta I_{RES\%}$	**L2B** $\Delta I_{RES\%}$	**L1B** $\Delta I_{RES\%}$	**L2B** $\Delta I_{RES\%}$	**L1B** $\Delta I_{RES\%}$	**L2B** $\Delta I_{RES\%}$
AlkB-Fe^{++} WT	52.6±2.0 %	39.0±1.02 %	+4.7±1.3 %	+1.7±1.2 %	+4.6±1.3 %	+2.1±1.0 %	+4.9±1.0 %	+1.7±1.0 %
AlkB-Fe^{++} N120 D	55.0±1.1 %	39.3±1.24 %	/	/	/	/	/	/

Table S2 | Kinetic parameters for ligand binding to AlkB-Fe^{++}. All data were collected in 150 mM NaCl, 15 mM Tris.HCl pH 8.0 at 28˚C. Errors are given as standard deviations. Proteins and ligands were added to the *cis* chamber.

	2-OG	**SUC**	**N-OG**
k_{off}^{-60mV} (s^{-1})	0.66±0.33	16.6±2.6	0.57±0.10
k_{on}^{-60mV} ($s^{-1}M^{-1}$)	1.8±0.3 x 10^3	9.2±1.3 x 10^2	1.2±0.3 x 10^3

Table S3 | $I_{RES\%}$ values of $DHFR_{tag}$:MTX ligand-induced current blockades. All data were collected at -90 mV applied potential in 150 mM NaCl, 15 mM Tris.HCl pH 7.5 at 28˚C. Values were calculated from at least 15 individual $DHFR_{tag}$:MTX blockades. Errors are given as standard deviations. The ClyA-AS open-pore conductance (I_o) was 1.6±0.1 nSi (N=15 single channels). $\Delta I_{RES\%}$ is the difference between the $I_{RES\%}$ of the $DHFR_{tag}$:MTX blockades and the $I_{RES\%}$ induced by the ligand (L1B or L2B). 50 nM of $DHFR_{tag}$ and 400 nM MTX were added to the *cis* chamber, NADPH and NADP+ were added to the *trans* chamber.

	No ligand		**NADP+**		**NADPH**	
	L1 $I_{RES\%}$	**L2** $I_{RES\%}$	**L1B** $\Delta I_{RES\%}$	**L2B** $\Delta I_{RES\%}$	**L2B** $\Delta I_{RES\%}$	**L2B** $\Delta I_{RES\%}$
$DHFR_{tag}$:MTX	74.7±0.5 %	53.5±0.9 %	+2.3±0.5 %	+4.7±0.9 %	+2.7±0.7 %	+5.4±1.0 %

Table S4 | Kinetic parameters for ligand binding to $DHFR_{tag}$:MTX. All data were collected in 150 mM NaCl, 15 mM Tris.HCl pH 7.5 at 28˚C. Errors are given as standard deviations. 50 nM of $DHFR_{tag}$ and 400 nM MTX were added to the *cis* chamber, NADPH and NADP+ were added to the *trans* chamber.

	NADP+	**NADPH**
k_{off}^{-90mV} (s^{-1})	10±1	NA
k_{on}^{-90mV} ($s^{-1}M^{-1}$)	2.1±0.3 x 10^6	4.8±1.2 x 10^6

Table S5 | Primer and aptamer sequences.

Primer name	Sequence
fAlkB	AGATATAGCCATGGCGTTGGATCTGTTTGCCGATGCTGAAC
AlkBr1	CGGATGGCTCCACGCGCTGCCTTCTTTTTTACCTGCCTGACGGAATG
AlkBr2	TATATATAAGCTTATCATTTTTCAAACTGCGGATGGCTCCACGCGCTGCC
120D	GCCAGATGCTTGTCTTATCAACCGCTACGCTCCTGGCGCGAAACTGTCGC
T7-terminator	GCTAGTTATTGCTCAGCGG
Anti-AlkB aptamer	TGCCTAGCGTTTCATTGTCCCTTCTTATTAGGTGATAATA
DHf	atatatatatCCATGGCTTCGGCTATGATTTCTCTGATTGCG
DHr	CGCGGTTTCTTTCGCTCGAGTACTGCTGCCacggcgttccaggatttcgaatgag
Cof	ctcattcgaaatcctggaacgccgtGGCAGCAGTACTCGAGCGAAAGAAACCGCG
Cor	atatatatatAAGCTTATCATTTTTCAAACTGCGGATGGC
dcr	atatatatatCTCGAGTACTGCTGCCACGGCGTTCCAGGATTTCG
delF	atatatatatCTCGAgcgggcAGCGCGTGGAGCCATCCGCAGTTTG
2dcF	atatatatatCTCGAGCGaagaagattgcggccctaaaacaggg
dcf	atatatatatCTCGAGCGaaaaagaagattgcggccctaaaacaggg

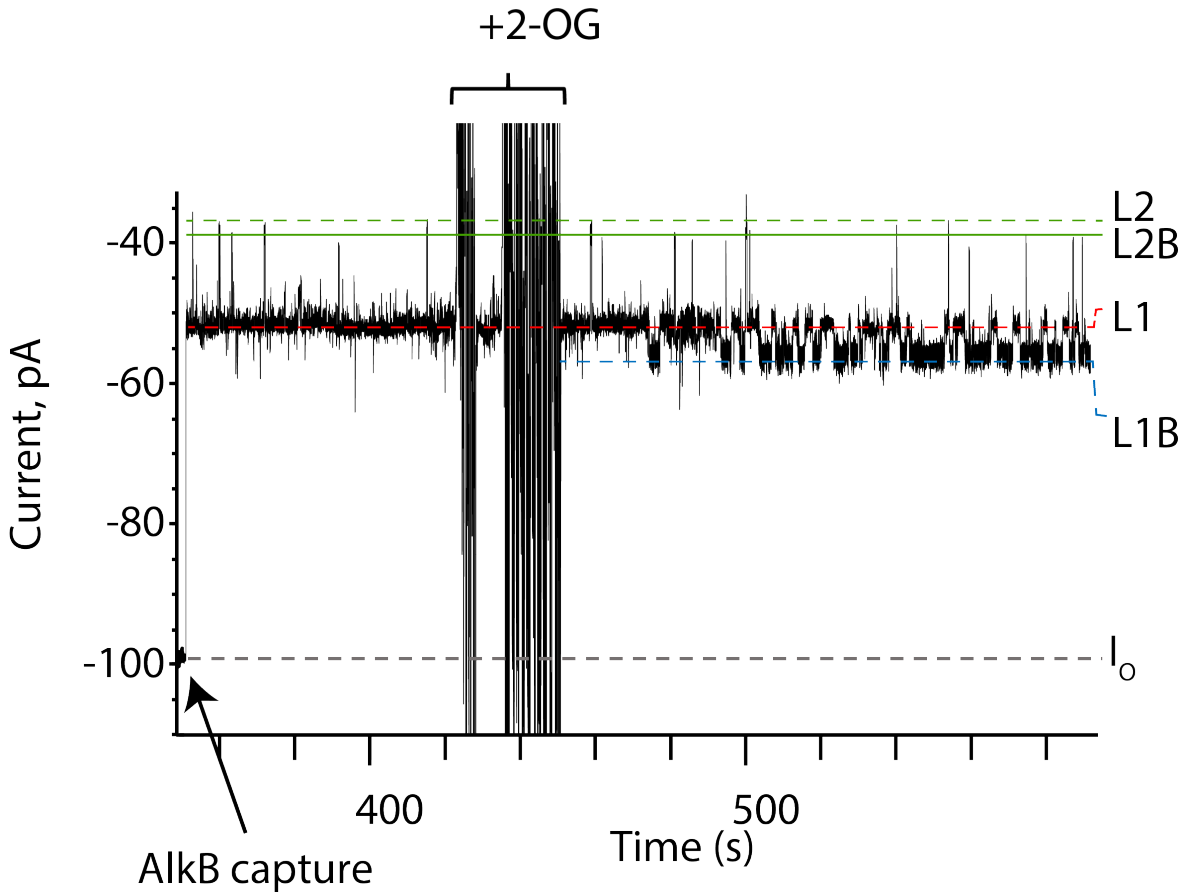

Figure S1. 2-OG induced binding events to a single AlkB-Fe^{++} molecule. The current trace shows the capture of an AlkB-Fe^{++} molecule (arrow) previously added to the *cis* compartment followed by the addition of 2-OG to the *cis* compartment. Confined AlkB-Fe^{++} showed L1 (dashed red line) and L2 (dashed green line) current levels, while 2-OG binding induced L1B (blue dashed line) and L2B (green line) ionic current levels. The grey dashed line corresponds to the open pore current (I_o). The trace was recorded at -60 mV applied potential in 150 mM NaCl, 15 mM Tris.HCl pH 8.0 at 28˚C using 2 kHz filtering and 10 kHz sampling rate, and filtered digitally with a Bessel (8-pole) low-pass filter with 50 Hz cut-off.

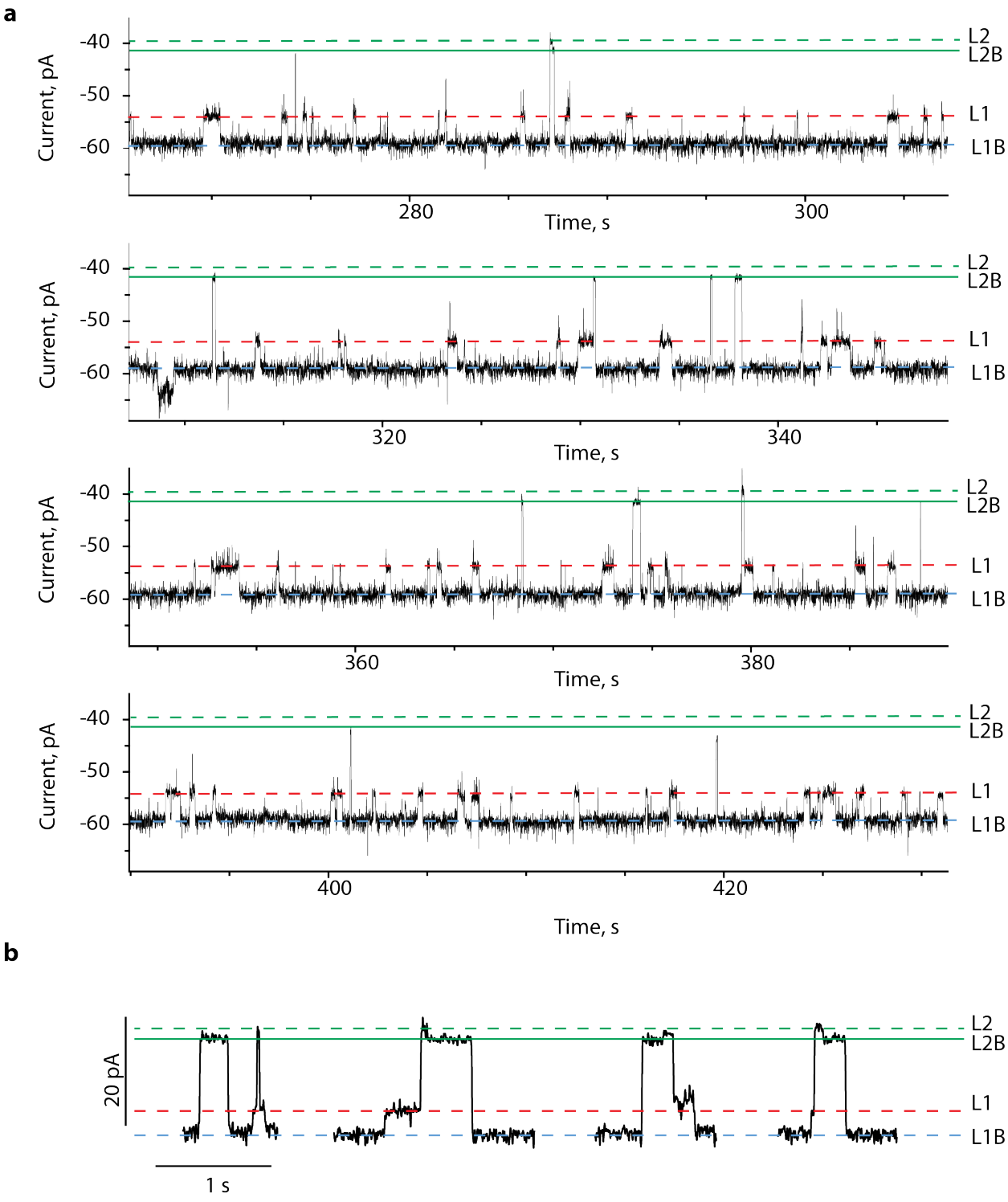

Figure S2. 2-OG induced current levels to AlkB-Fe^{++}. a, Extended current trace showing L1 (red dashed line), L1B (blue dashed line), L2 (green dashed line) and L2B (green line) current levels induced by the binding of 2-OG to a single confined AlkB-Fe^{++}. **b,** Selected traces

showing the details of the ligand-induced current levels. Transitions were always from L1B to L2B or from L1 to L2, or from L2 to L1 or from L2B to L1B. Current traces were recorded in presence of 4.8 mM 2-OG at -60 mV applied potential in 150 mM NaCl, 15 mM Tris.HCl pH 8.0 at 28˚C using 2 kHz filtering and 10 kHz sampling rate, and filtered digitally with a Bessel (8-pole) low-pass filter with 50 Hz cut-off.

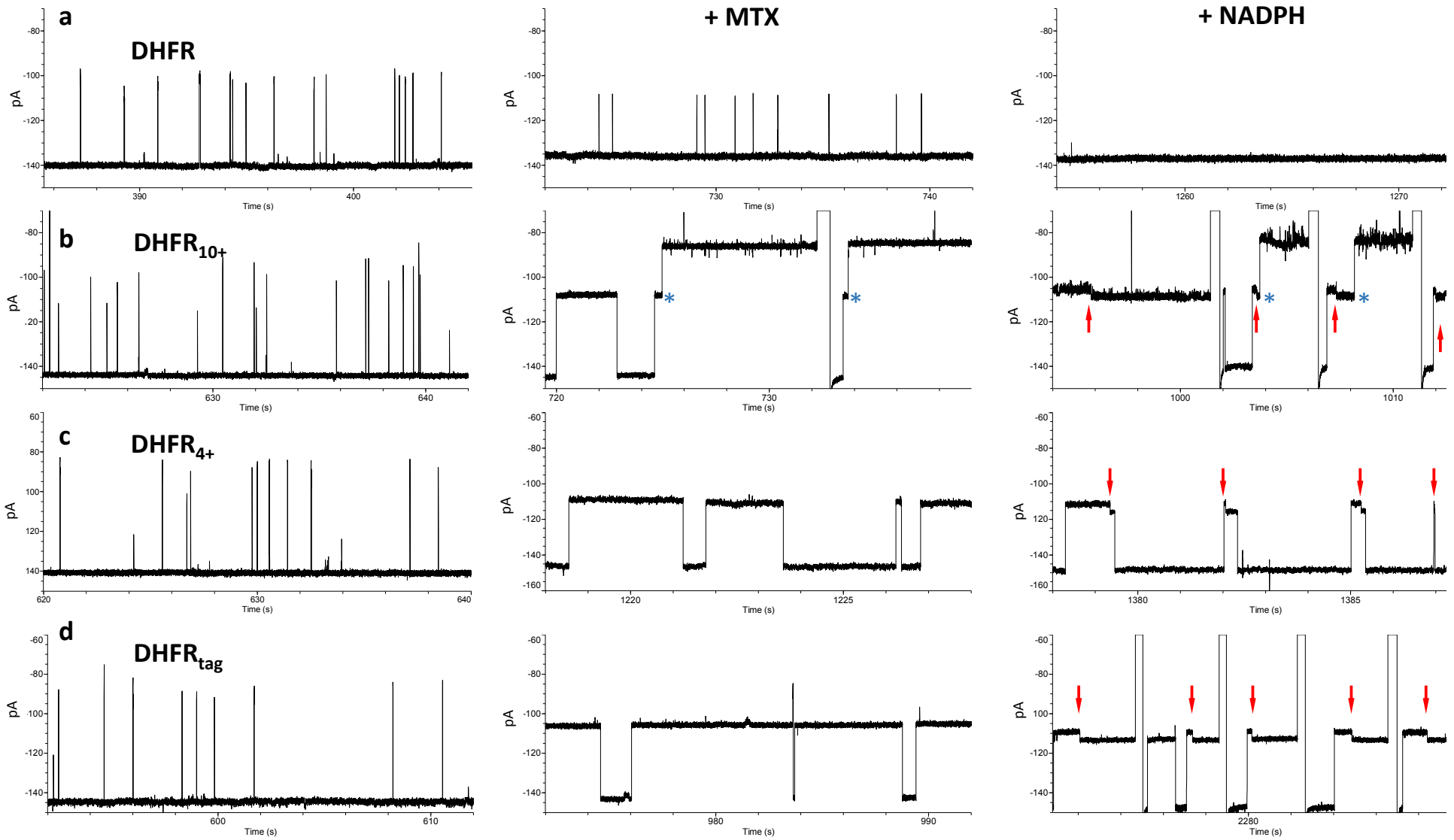
a
DHFR
b
DHFR10+
c
DHFR4+
d
DHFRtag
+ MTX
+ NADPH
pA
Time (s)

Figure S3. $DHFR_{n+}$, $DHFR_{n+}$:MTX and $DHFR_{n+}$:MTX:NADPH induced current blockades to ClyA-AS nanopores. Representative traces recorded in presence of ~50 nM of **a:** DHFR, **b**: $DHFR_{10+}$, **c**: $DHFR_{4+}$, **d**: $DHFR_{tag}$ added to the *cis* compartment. Every set of three panels shows $DHFR_{n+}$ blockades recorded without ligands (**left**), after the addition of 400 nM MTX to the *cis* compartment (**centre**) and after further addition of 20 μM of NADPH in *cis* (**a**) or 0.7 μM of NADPH to the *trans* compartment (**b,c,d**) (**right**). The red arrows indicate NADPH binding events to the binary $DHFR_{n+}$:MTX complexes. The blue asterisks indicate the transition of $DHFR_{10+}$:MTX to a lower conductance level. Current traces were recorded at -90 mV applied potential in 150 mM NaCl, 15 mM Tris.HCl pH 7.5 at 28˚C using 2 kHz filtering and 10 kHz sampling rate, and filtered digitally with a Gaussian low-pass filter with 500 Hz cut-off.

>DHFR$_{10+}$

```
        * **     * **    *     *     * *     * *     ***     *
ERRGSSTRAKETAAAKFERQHMDSGSAKIAALKQKIAALKYKNAALKKKIAALKQGSAWSHPQF
**
EK**
```

>DHFR$_{tag}$

```
        * ***     *            **
ERRGSSTRAKKKIAALKQGSAWSHPQFEK**
```

>DHFR$_{4+}$

```
        * **     *            **
ERRGSSTRAKKIAALKQGSAWSHPQFEK**
```

>DHFR

```
        *           **
ERRGSSTRAGSAWSHPQFEK**
```

Figure S4. Sequences of the DHFR constructs used in this work. The C-terminus of DHFR, the sequences of the S-tag, the positive coil and the Strep-tag are colored green, gray, cyan and yellow, respectively. The sequences of the flexible linkers are underlined. The positively charged amino acids in the polypeptide tags are indicated by a blue asterisk and the negatively charged amino acids by a red asterisk.

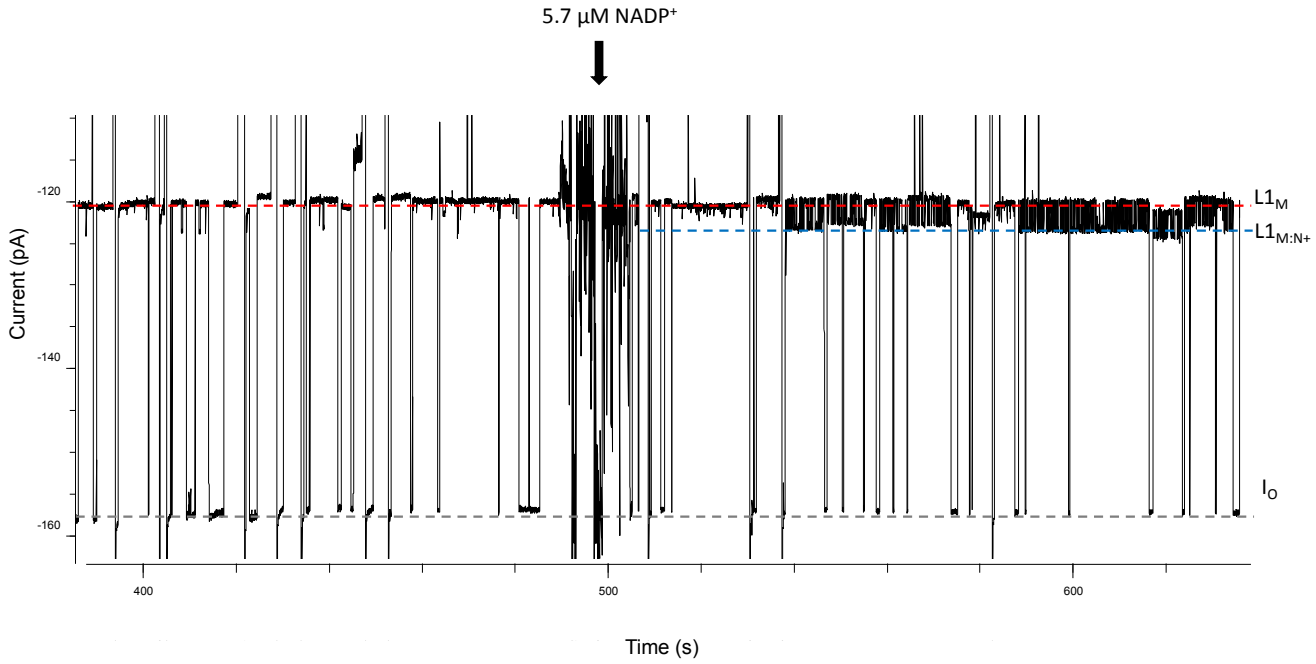

Figure S5 | NADP+ induced binding events to $DHFR_{tag}$:MTX. The current trace shows $DHFR_{tag}$:MTX (added to the *cis* compartment, 50 nM of $DHFR_{tag}$ and 400 nM MTX) blockades before (left) and after (right) the addition of 5.7 µM NADP+ (arrow) to the *trans* compartment. The binding of NADP+ results in reversible current enhancements from $L1_M$ (red dashed line) to $L1_{M:N+}$ (blue dashed line). The grey dashed line corresponds to the open pore current (I_o). The trace was recorded at -90 mV applied potential in 150 mM NaCl, 15 mM Tris.HCl pH 7.5 at 28˚C using 2 kHz filtering and 10 kHz sampling rate, and filtered digitally with a Bessel (8-pole) low-pass filter with 50 Hz cut-off.

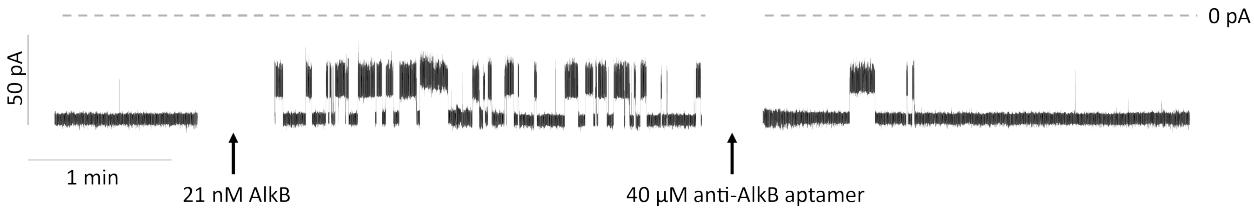

Figure S6. Effect of the cognate Anti-AlkB aptamer on the AlkB-Fe^{++}-induced current blockades.

The addition of 40 µM cognate aptamer (TGCCTAGCGTTTCATTGTCCCTTCTTATTAGGTGATAATA, Table S5) reduced the frequency of the AlkB-Fe^{++} blockades to ClyA-AS caused by 21 nM AlkB-Fe^{++} due to electrostatic repulsion and/or steric hindrance between the AlkB:aptamer complexes and the negatively charged ClyA-AS lumen.[2] The recordings were carried out in 150 mM NaCl, 15 mM Tris HCl pH 8.0 at 28˚C and at -35 mV applied potential.

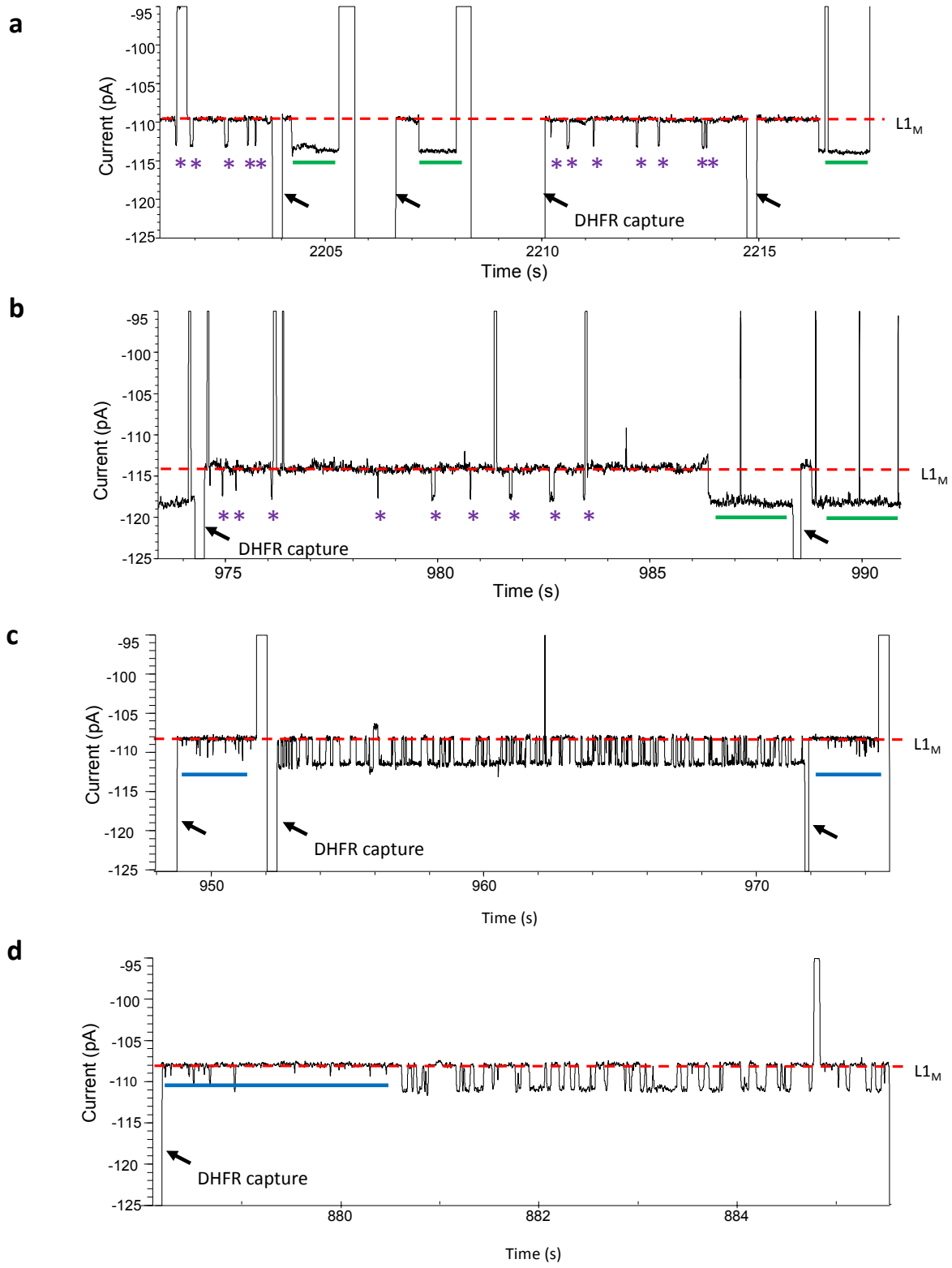
a
b
c
d
Current (pA)
Time (s)
L1M
DHFR capture
-95
-100
-105
-110
-115
-120
-125
2205
2210
2215
975
980
985
990
950
960
970
880
882
884

Figure S7. Heterogeneity of NADPH and NADP+ binding to $DHFR_{tag}$:MTX. a,b The current traces show the capture of $DHFR_{tag}$:MTX inside ClyA-AS (50 nM of $DHFR_{tag}$ and 400 nM of MTX added to the *cis* compartment), after the addition of 0.74 μM NADPH to the *trans* compartment. The red dashed line represents the $DHFR_{tag}$:MTX $L1_M$ level. The purple asterisks indicate "short" (*i.e.* low affinity) NADPH binding events, while the green lines indicate "long" (*i.e.* high affinity) NADPH induced binding events. The arrows show the capture of a new $DHFR_{tag}$:MTX complex. The current trace in (**a**) shows $DHFR_{tag}$:MTX blockades displaying either "short" or "long" NADPH binding events. The current trace in (**b**) shows the switching between "short" and "long" binding modes within the same $DHFR_{tag}$:MTX blockade. **c,d** $DHFR_{tag}$:MTX blockades (50 nM $DHFR_{tag}$ and 400 nM MTX in *cis*) after the addition of 5.7 μM NADP+ in *trans*. The red dashed line represents the $DHFR_{tag}$:MTX $L1_M$ level, the non-responsive state of the binary complex towards NADP+ is indicated by a blue line. The arrows indicate the capture of a new $DHFR_{tag}$:MTX complex. The current trace in (**c**) shows $DHFR_{tag}$:MTX blockades that are either responsive or non-responsive towards NADP+ addition. The current trace in (**d**) shows the switching between non-responsive and responsive states within the same $DHFR_{tag}$:MTX blockade. The traces were recorded at -90 mV applied potential in 150 mM NaCl, 15 mM Tris.HCl pH 7.5 at 28˚C using 2 kHz filtering and 10 kHz sampling rate, and filtered digitally with a Bessel (8-pole) low-pass filter with 50 Hz cut-off.

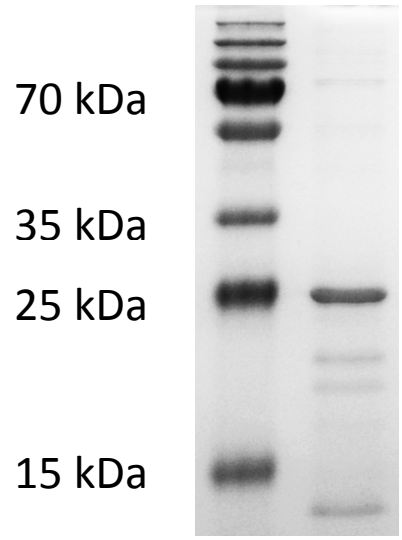

Figure S8. Purity of the strep-tagged purified wild type AlkB-Fe^{++} assayed by a 12 % SDS PAGE. Left lane: protein marker (Page Ruler Plus Prestained Protein Ladder, Thermo scientific). Right lane: ~5 µg of the purified AlkB-Fe^{++}.

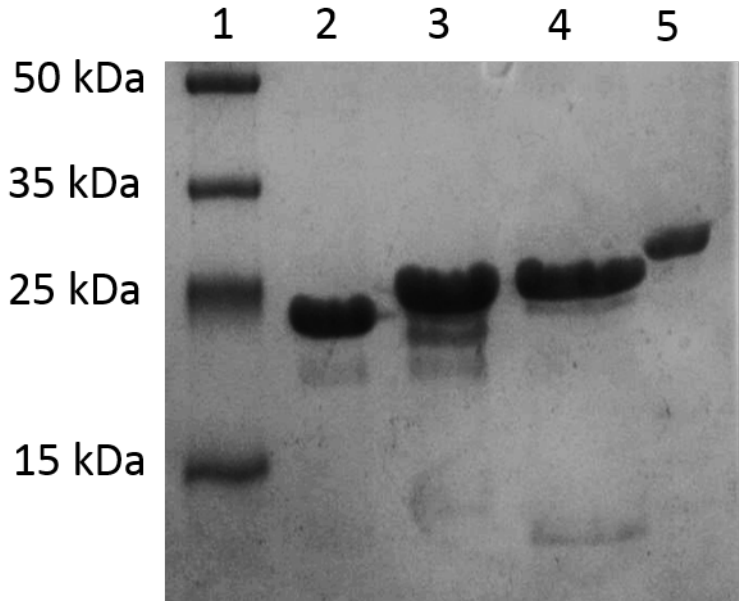

Figure S9. Purity of the strep-tagged purified $DHFR_{n+}$ assayed by a 15 % SDS PAGE. Lane 1: protein marker (Page Ruler Plus Prestained Protein Ladder, Thermo scientific). Lanes 2-5: ~5 µg of purified DHFR (lane 2), $DHFR_{4+}$ (lane 3), $DHFR_{tag}$ (lane 4) and ~10 µg of purified $DHFR_{10+}$ (lane 5).

References

(1) Welford, R. W.; Schlemminger, I.; McNeill, L. A.; Hewitson, K. S.; Schofield, C. J. *The Journal of biological chemistry* **2003**, *278*, 10157.

(2) Soskine, M.; Biesemans, A.; Moeyaert, B.; Cheley, S.; Bayley, H.; Maglia, G. *Nano Letters* **2012**, *12*, 4895.

(3) Franceschini, L.; Soskine, M.; Biesemans, A.; Maglia, G. *Nature Communications* **2013**, *4*, 2415.

(4) Krylova, S. M.; Karkhanina, A. A.; Musheev, M. U.; Bagg, E. A.; Schofield, C. J.; Krylov, S. N. *Anal Biochem* **2011**, *414*, 261.

(5) Rajagopalan, P. T.; Zhang, Z.; McCourt, L.; Dwyer, M.; Benkovic, S. J.; Hammes, G. G. *Proceedings of the National Academy of Sciences of the United States of America* **2002**, *99*, 13481.

(6) Soskine, M.; Biesemans, A.; De Maeyer, M.; Maglia, G. *J Am Chem Soc* **2013**, *135*, 13456.

(7) Thomas, F.; Boyle, A. L.; Burton, A. J.; Woolfson, D. N. *J Am Chem Soc* **2013**.

(8) Bleijlevens, B.; Shivarattan, T.; van den Boom, K. S.; de Haan, A.; van der Zwan, G.; Simpson, P. J.; Matthews, S. J. *Biochemistry* **2012**, *51*, 3334.

(9) Ergel, B.; Gill, M. L.; Brown, L.; Yu, B.; Palmer, A. G., 3rd; Hunt, J. F. *The Journal of biological chemistry* **2014**, *289*, 29584.

(10) Zhang, Z.; Rajagopalan, P. T.; Selzer, T.; Benkovic, S. J.; Hammes, G. G. *Proceedings of the National Academy of Sciences of the United States of America* **2004**, *101*, 2764.

(11) Bleijlevens, B.; Shivarattan, T.; Flashman, E.; Yang, Y.; Simpson, P. J.; Koivisto, P.; Sedgwick, B.; Schofield, C. J.; Matthews, S. J. *EMBO reports* **2008**, *9*, 872.

(12) Schnell, J. R.; Dyson, H. J.; Wright, P. E. *Annual review of biophysics and biomolecular structure* **2004**, *33*, 119.

(13) Gianni, S.; Dogan, J.; Jemth, P. *Biophysical chemistry* **2014**, *189*, 33.

(14) Iwakura, M.; Jones, B. E.; Luo, J.; Matthews, C. R. *J Biochem* **1995**, *117*, 480.

(15) Miles, G.; Cheley, S.; Braha, O.; Bayley, H. *Biochemistry* **2001**, *40*, 8514.

(16) Miyazaki, K. *Methods Enzymol* **2011**, *498*, 399.